

CORRELATED VARIABILITY IN THE BLAZAR 3C 454.3

E. W. BONNING¹, C. BAILYN², C. M. URRY¹, M. BUXTON², G. FOSSATI⁴, L. MARASCHI³, P. COPPI², R. SCALZO¹, J. ISLER¹, A. KAPTUR²

Submitted to ApJ Letters

ABSTRACT

The blazar 3C 454.3 was revealed by the Fermi Gamma-ray Space Telescope to be in an exceptionally high flux state in July 2008. Accordingly, we performed a multi-wavelength monitoring campaign on this blazar using IR and optical observations from the SMARTS telescopes, optical, UV and X-ray data from the Swift satellite, and public-release gamma-ray data from Fermi. We find an excellent correlation between the IR, optical, UV and gamma-ray light curves, with a time lag of less than one day. The amplitude of the infrared variability is comparable to that in gamma-rays, and larger than at optical or UV wavelengths. The X-ray flux is not strongly correlated with either the gamma-rays or longer wavelength data. These variability characteristics find a natural explanation in the external Compton model, in which electrons with Lorentz factor $\gamma \sim 10^{3-4}$ radiate synchrotron emission in the infrared-optical and also scatter accretion disk or emission line photons to gamma-ray energies, while much cooler electrons ($\gamma \sim 10^{1-2}$) produce X-rays by scattering synchrotron or other ambient photons.

Subject headings: galaxies: active — quasars: general — black hole physics — BL Lacertae objects: individual (3C 454.3)

1. INTRODUCTION

Blazars are understood to be active galactic nuclei (AGN) with aligned relativistic jets (Urry & Padovani 1995), so they offer a unique laboratory for studying the physics of astrophysical jets. The spectral energy distributions (SEDs) of blazars have a characteristic double-humped shape with a low-energy component peaking anywhere from radio to X-rays, and a high-energy component peaking at MeV to GeV energies (Fossati et al. 1998). Flat Spectrum Radio Quasars (FSRQs) like 3C 454.3 have SED peaks at radio-IR wavelengths and ~ 1 GeV (Urry & Padovani 1995; Sambruna et al. 1996). The low-energy component is well modeled as synchrotron emission from relativistic electrons in the jet (Konigl 1981; Urry & Mushotzky 1982), while the origin of the second SED peak at high energies is not fully understood. Current explanations for the gamma-ray emission fall into two categories, leptonic and hadronic. Leptonic models produce high-energy flux by inverse-Compton scattering of low-energy seed photons, either the synchrotron photons themselves (Synchrotron Self-Compton, Jones et al. 1974) or photons from an external source, such as thermal accretion disk emission or broad-line emission (Sikora et al. 1994; Dermer & Schlickeiser 1993; Ghisellini & Madau 1996; Celotti & Ghisellini 2008). In hadronic models, protons that are accelerated to very high energies in the jet produce gamma-rays from neutral pion decay, proton synchrotron

emission, and synchrotron emission from pair production (Mücke & Protheroe 2001; Mücke et al. 2003; Böttcher 2007). Both leptonic and hadronic models can adequately fit single-epoch blazar SEDs, but variability offers a test of either model.

3C 454.3 was among the more intense and variable FSRQs detected with CGRO EGRET (Hartman et al. 1999), varying over several years by factors of up to five, with a flare-state flux of $F_{>100 \text{ MeV}} \sim 0.5 \times 10^{-6}$ photons/s/cm² (Hartman et al. 1993, 1999; Aller et al. 1997). Long-term optical variability has also been reported, with up to ~ 3 mag changes over several years Djorgovski et al. (2008). During a 2005 optical flare to R=12 (Villata et al. 2006), 3C 454.3 was detected with INTEGRAL at a flux of $F_{3-200 \text{ keV}} \sim 3 \times 10^{-2}$ photons/s/cm² (Pian et al. 2006); a radio flare followed about a year later (Villata et al. 2007). 3C 454.3 has been detected with the AGILE gamma-ray satellite (Tavani et al. 2008), flaring in July 2007 and again in July 2008 (Vercellone et al. 2008; Gasparri et al. 2008) with associated flaring at optical and longer wavelengths (Ghisellini et al. 2007; Villata et al. 2008). On 24 July 2008, Tosti et al. (2008) confirmed the high gamma-ray flux state of the source with a detection by the Fermi Large Area Telescope (LAT) while still in its post-launch commissioning phase. In the Fermi/LAT first light image released on 26 August 2008, 3C 454.3 was among the brightest sources in the gamma-ray sky, at the high end of its recorded gamma-ray intensity, $F_{0.1-300 \text{ GeV}} \sim 4.4 \times 10^{-6}$ photons/s/cm².

Here we present data from our multi-wavelength optical and infrared monitoring program of 3C 454.3 from June to December 2008 with the Small and Moderate Aperture Research Telescope System (SMARTS). We correlate these data with Target of Opportunity observations carried out with the Swift X-ray Telescope (XRT) and Ultraviolet and Optical Telescope (UVOT), as well

¹ Department of Physics and Yale Center for Astronomy and Astrophysics, Yale University, PO Box 208121, New Haven, CT 06520-8121; erin.bonning@yale.edu

² Department of Astronomy and Yale Center for Astronomy and Astrophysics, Yale University, PO Box 208101, New Haven, CT 06520-8101

³ INAF - Osservatorio Astronomico di Brera, V. Brera 28, I-20100 Milano, Italy

⁴ Department of Physics and Astronomy, Rice University, Houston, TX 77005

as with 0.1–300 GeV fluxes made public by the Fermi Science Support Center. The observations are described in Section 2. The light curves, correlation functions, and SED are discussed in Section 3.

2. OBSERVATIONS

2.1. SMARTS

Photometric monitoring of 3C 454.3 was carried out on the 1.3m telescope located at Cerro Tololo Interamerican Observatory (CTIO) with the ANDICAM instrument. ANDICAM is a dual-channel imager with a dichroic that feeds an optical CCD and an IR imager, which can obtain simultaneous data from 0.4 to 2.2 μ . Our campaign began with observations in B, V, R and J-bands with a cadence of one observation every 2 nights. After it became clear that 3C 454.3 was exhibiting interesting and varied behavior, we added K-band observations and increased the cadence to one observation every night. The SMARTS photometric data and light curves for 3C 454.3 as well as all other Fermi/LAT monitored blazars visible from CTIO are made publicly available on a 1-2 day timescale on the web.⁵

Optical data were bias-subtracted, overscan-subtracted, and flat fielded using *ccdproc* in IRAF. The optical photometry was calibrated using published magnitudes of a secondary standard star⁶ in the field of 3C 454.3 (Craine 1977; Angione 1971; Fiorucci et al. 1998). Infrared data were sky-subtracted, flat fielded, and dithered images combined using in-house IRAF scripts. The infrared photometry was calibrated using 2MASS magnitudes of a secondary standard star (the same star used in optical photometry calibration) in the field of 3C 454.3. We estimated photometric errors by calculating the 1- σ variation in magnitude of comparison stars with comparable magnitude to 3C 454.3. These are as follows: $B_{\text{err}} = 0.02$ mag, $V_{\text{err}} = 0.02$ mag, $R_{\text{err}} = 0.02$, $J_{\text{err}} = 0.04$ mag, and $K_{\text{err}} = 0.04$ mag.

Figure 3 shows the B-band light curve normalized to its flux at JD 2454700. Figure 3 shows two SEDs for 3C 454.3: one averaged over the actively flaring period up to JD 2454750, and a second averaged over the relatively quiescent period after that day. To compute the fluxes, magnitudes were dereddened using the extinction relations in Cardelli et al. (1989) together with the value for A_B given by Schlegel et al. (1998) and converted into flux densities using the zero-point fluxes given by Bessell et al. (1998) and Beckwith et al. (1976)

2.2. Fermi

The Fermi Space Telescope (formerly GLAST) was launched on 11 June 2008. The Fermi observatory Large Area Telescope (LAT) is designed to measure the cosmic gamma-ray flux up to ~ 300 GeV. The LAT is an imaging, wide field-of-view high-energy pair conversion telescope with energy range from ~ 20 MeV to $\gtrsim 300$ GeV, and surveys the sky every three hours (Michelson 2007). As a service to the community and in order to support correlated multiwavelength observations, the LAT Instrument Science Operations Center provides daily and weekly averaged fluxes for a number of blazars, of which

3C 454.3 is one. Fluxes and 1σ uncertainties for three bands, 0.1–300 GeV, 0.3–1 GeV, and 1–300 GeV, using preliminary instrument response functions and calibrations, are made available online roughly once per week, with the caveat that the early flux estimates are not absolutely calibrated, and may have variations of up to 10% due to uncorrected systematic effects. Because the observed variations are well correlated with independently measured IR, optical, and UV variations, we conclude the gamma-ray variations will not change significantly even if they are eventually recalibrated, and in any case, our key results are robust against 10% fluctuations in gamma-ray intensity. We show the 3C 454.3 light curve in the 0.1–300 GeV band in Figure 3 normalized to its photon flux at JD 2454700. Fluxes shown in Figure 3 are computed from the publicly released data in the 0.3–1 GeV and 1–300 GeV bands by assuming a power-law spectrum of photon index $\Gamma=2$.

2.3. Swift

Since being identified in June 2008 as an extraordinarily bright gamma-ray source (Vitorini et al. 2008; Gasparrini et al. 2008), 3C 454.3 has been the subject of numerous Swift target of opportunity observations, including one by PI Bonning covering 22 September - 02 October, 2008. The Swift satellite (Gehrels et al. 2004) has three instruments: a coded-mask Burst Alert Telescope (BAT, Barthelmy et al. 2005), an X-ray Telescope covering the energy range 0.2–20 keV (XRT, Burrows et al. 2005), and an Ultraviolet/Optical Telescope covering 170–600 nm (UVOT, Roming et al. 2005). Swift data are made public to the community within a few days of the observations; therefore we were able to collect all available data within the period of our SMARTS observations. We reduced the data from the X-ray telescope (XRT) and the Ultraviolet Optical Telescope (UVOT) according to the standard recipes given by the Swift data analysis manuals.

For each obsid, the UVOT data for each exposure were co-added with the task *wvotimsum*. The source magnitudes were then computed from a source region of 5.5 arcsec using the task *wvotsource*, which performs aperture photometry on the source and returns the count rate, flux density, and magnitude in the Swift/UVOT photometric system (Poole et al. 2008). We correct these for interstellar extinction as described in Section 2.1. Light curves from the UVOT B and W1 bands are shown in Figure 3, and average fluxes before and after JD 2454750 in Figure 3.

For each obsid, the XRT level-2 event list was generated via *xrtpipeline v. 0.11.5* with the default filtering and screening criteria, selecting photon counting (PC) data with XRT event grades 0-12. We extracted the source spectrum from a region centered at the source with a radius of 60 arcsec and subtracted the background from a nearby source-free region. Spectra were rebinned to 25 cts/bin, fit with an absorbed power law, and the flux was computed in 0.5 – 2.0 keV and 2.0 – 10.0 keV bands. The X-ray light curve is shown in the bottom panel of Figure 3.

3. RESULTS AND DISCUSSION

The correlated variability across all observed wavebands except the X-ray is readily apparent in Figure 3.

⁵ <http://astro.yale.edu/glast/index.html>

⁶ Shown as star H in the finding chart at <http://www.lsw.uni-heidelberg.de/projects/extragalactic/charts/2251+158.html>

All observed bands save the X-ray show two prominent peaks around JD 2454715 and a short flare near JD 2454740. The amplitude is largest in the gamma-rays and J band. Figure 2 shows the discrete correlation function (DCF, Edelson & Krolik 1988; White & Peterson 1994) calculated for the gamma-ray (0.1–300 GeV) flux versus light curves in the optical B band⁷, which has the best temporal coverage, and infrared J-band, which shows the strongest variations. The DCF shows a peak correlation amplitude ~ 0.7 at $\tau = 0$, indicating no detectable lag between IR/optical and gamma-ray fluxes. Given the sampling, this means any lag is less than or about 1 day. Similar results were reported by Vercellone et al. (2009) for the earlier flare observed with AGILE, though with much lower significance. The optical versus IR DCF shows even stronger correlation (amplitude ~ 0.8), also with 0 ± 1 day lag.

Table 1 shows the fractional root mean square (rms) variability amplitude (Vaughan et al. 2003) for each band. The IR, optical, and UV variability amplitudes decrease toward shorter wavelengths, suggesting the possible presence of steady thermal emission (UV accretion disk emission plus Balmer continuum, Fe II, and Mg II in the V and B bands) added to the steeper-spectrum jet. Evidence for ‘big’ and ‘little’ blue bumps was found previously in the SED of 3C 454.3 during periods of low emission (Raiteri et al. 2007). The colors of 3C 454.3 are redder at brighter levels, historically (Villata et al. 2006) and in the present data, also supporting the presence of thermal emission beneath the much brighter non-thermal jet.

The closely correlated IR/gamma-ray variability of 3C 454.3 supports a model in which relativistic electrons in the jet radiate IR/optical synchrotron photons and inverse Compton scatter thermal photons to X- and gamma-ray energies. The observed gamma-ray flares must be caused by changes in the injection luminosity of the higher energy electrons, rather than variability of the ambient thermal photons, since in that case there would be higher amplitude variations in the UV than the infrared. The implication of the short lag time (Fig. 2) is that electrons of similar energy produce IR and gamma-ray emission.

Figure 3 shows the SED in the high state (JD 2454680–2454750) and at the lower final intensity (JD 2454750–2454820). The SED of the high flux state prior to JD 2454750 shows an optical/IR flux level similar to that of the May 2007 flare (Raiteri et al. 2008), intermediate between the high and low states reported by Raiteri et al. (2007) (and references therein), so not surprisingly, the basic model parameters are similar. The optical/UV emission is due to the highest energy electrons (Lorentz factors $\sim 10^{3-4}$) radiating via synchrotron in a field of ~ 10 Gauss, while the gamma-rays come from inverse Compton scattering on the broad-line photons. The bulk Lorentz factor is $\Gamma \sim \delta \sim 10 - 15$ (where $\delta = [\gamma(1 - \beta \cos \theta)]^{-1}$ is the Doppler beaming factor).

The lack of correlation seen in the DCF for 2–10 keV X-rays with respect to the other wavebands finds a natural explanation in the external Compton scenario, with the

X-rays coming from low-energy electrons ($\gamma \sim 10-100$) inverse-Compton scattering external UV photons, rather than higher energy electrons ($\sim 10^{3-4}$) scattering synchrotron photons. An SSC component in X-rays would introduce correlation between X-rays and gamma-rays, which is not seen. The highest energy electrons (producing the IR/optical and gamma-ray emission) vary more rapidly (the radiative timescales are shorter) while the low energy electrons act as a reservoir and vary more slowly.

More precise SED modeling is needed to determine detailed model parameters, such as the energy density and location of the thermal photons, the location and size of the scattering region, the electron distribution, the bulk Lorentz factor and jet orientation, etc. This detailed analysis will be deferred to a later paper. Still, some additional conclusions can be made. The overall stability of source parameters and the correlation imply that the emission region is stable on time scales of ~ 1 month. If the electrons are localized in a fast moving knot (which might become visible in VLBI maps in a few months), it moves a distance $\gamma^2 c \Delta t$, roughly 1-10 pc, i.e., the jet parameters cannot change dramatically on this scale. However, the Sikora et al. (1994) model for 3C 454.3 can be ruled out as the source of the rapid variations discussed here, since their assumed source size of 10^9 cm implies $\Delta t \gtrsim 1$ year. Instead, their model might explain a slowly changing, much larger region of the jet.

In conclusion, 3C 454.3 shows very strong, correlated variability between the peak of the synchrotron component (at infrared, optical and UV wavelengths) and the peak of the gamma-ray component. No such correlation is seen between X-rays and any other band. These results suggest that the variability arises from changes in the electron luminosity at a compact location in the jet. The highly variable infrared through UV emission, particularly in the brightest state, is dominated by synchrotron emission from a compact region of high-energy electrons in the jet, with a smaller contribution from a relatively steady accretion disk. The slowly varying low-energy part of the electron spectrum gives rise to relatively stable X-ray emission via scattering. The gamma-rays vary in a correlated way because they result from the same high-energy electrons up-scattering ambient UV photons.

SMARTS observations of LAT-monitored blazars are supported by Fermi GI grant 011283. CDB, MMB and the SMARTS 1.3m observing queue also receive support from NSF grant AST-0707627. This research has made use of the NASA/IPAC Infrared Science Archive, which is operated by the Jet Propulsion Laboratory, California Institute of Technology, under contract with the National Aeronautics and Space Administration.

⁷ For the B band, we include optical fluxes from both the Swift and SMARTS telescopes in order to have complete coverage over gaps in the individual light curves.

REFERENCES

- Aller, M. F. et al. 1997, in AIP Conference Series, Vol. 410, Proceedings of the Fourth Compton Symposium, ed. C. D. Dermer, M. S. Strickman, & J. D. Kurfess, 1423–+
- Angione, R. J. 1971, *AJ*, 76, 412
- Barthelmy, S. D. et al. 2005, *Space Science Reviews*, 120, 143
- Beckwith, S. et al. 1976, *ApJ*, 208, 390
- Bessell, M. S., Castelli, F., & Plez, B. 1998, *A&A*, 333, 231
- Böttcher, M. 2007, *Ap&SS*, 309, 95
- Burrows, D. N. et al. 2005, *Space Science Reviews*, 120, 165
- Cardelli, J. A., Clayton, G. C., & Mathis, J. S. 1989, *ApJ*, 345, 245
- Celotti, A. & Ghisellini, G. 2008, *MNRAS*, 385, 283
- Craine, E. R. 1977, *A handbook of quasistellar and BL Lacertae objects* (Astronomy and Astrophysics Series, Tucson: Pachart, 1977)
- Dermer, C. D. & Schlickeiser, R. 1993, *ApJ*, 416, 458
- Djorgovski, S. G. et al. 2008, *The Astronomer’s Telegram*, 1684, 1
- Edelson, R. A. & Krolik, J. H. 1988, *ApJ*, 333, 646
- Fiorucci, M., Tosti, G., & Rizzi, N. 1998, *PASP*, 110, 105
- Fossati, G. et al. 1998, *MNRAS*, 299, 433
- Gasparrini, D. et al. 2008, *The Astronomer’s Telegram*, 1592, 1
- Gehrels, N. et al. 2004, *ApJ*, 611, 1005
- Ghisellini, G. et al. 2007, *MNRAS*, 382, L82
- Ghisellini, G. & Madau, P. 1996, *MNRAS*, 280, 67
- Hartman, R. C. et al. 1999, *ApJS*, 123, 79
- Hartman, R. C. et al. 1993, *ApJ*, 407, L41
- Jones, T. W., O’dell, S. L., & Stein, W. A. 1974, *ApJ*, 188, 353
- Konigl, A. 1981, *ApJ*, 243, 700
- Michelson, P. F. 2007, in AIP Conference Series, Vol. 921, *The First GLAST Symposium*, ed. S. Ritz, P. Michelson, & C. A. Meegan, 8–12
- Mücke, A. & Protheroe, R. J. 2001, *Astroparticle Physics*, 15, 121
- Mücke, A. et al. 2003, *Astroparticle Physics*, 18, 593
- Pian, E. et al. 2006, *A&A*, 449, L21
- Poole, T. S. et al. 2008, *MNRAS*, 383, 627
- Raiteri, C. M. et al. 2007, *A&A*, 473, 819
- Raiteri, C. M. et al. 2008, *A&A*, 485, L17
- Roming, P. W. A. et al. 2005, *Space Science Reviews*, 120, 95
- Sambruna, R. M., Maraschi, L., & Urry, C. M. 1996, *ApJ*, 463, 444
- Schlegel, D. J., Finkbeiner, D. P., & Davis, M. 1998, *ApJ*, 500, 525
- Sikora, M., Begelman, M. C., & Rees, M. J. 1994, *ApJ*, 421, 153
- Tavani, M. et al. 2008, *Nuclear Instruments and Methods in Physics Research A*, 588, 52
- Tosti, G. et al. 2008, *The Astronomer’s Telegram*, 1628, 1
- Urry, C. M. & Mushotzky, R. F. 1982, *ApJ*, 253, 38
- Urry, C. M. & Padovani, P. 1995, *PASP*, 107, 803
- Vaughan, S. et al. 2003, *MNRAS*, 345, 1271
- Vercellone, S. et al. 2008, *ApJ*, 676, L13
- Vercellone, S. et al. 2009, *ApJ*, 690, 1018
- Villata, M. et al. 2007, *A&A*, 464, L5
- Villata, M. et al. 2006, *A&A*, 453, 817
- Villata, M. et al. 2008, *The Astronomer’s Telegram*, 1625, 1
- Vittorini, V. et al. 2008, *The Astronomer’s Telegram*, 1581, 1
- White, R. J. & Peterson, B. M. 1994, *PASP*, 106, 879

TABLE 1
FRACTIONAL VARIABILITY AMPLITUDE

Band	F_{var}
K	0.510 ± 0.0004
J	0.603 ± 0.0001
R	0.472 ± 0.001
V	0.385 ± 0.001
B	0.362 ± 0.001
U	0.193 ± 0.002
W1	0.165 ± 0.003
M2	0.142 ± 0.004
W2	0.140 ± 0.004
2-10 keV	0 ^a
0.1-300 GeV	0.455 ± 0.015

^aThe X-ray sample variance was equivalent to the mean square error, leading to a value of F_{var} consistent with zero.

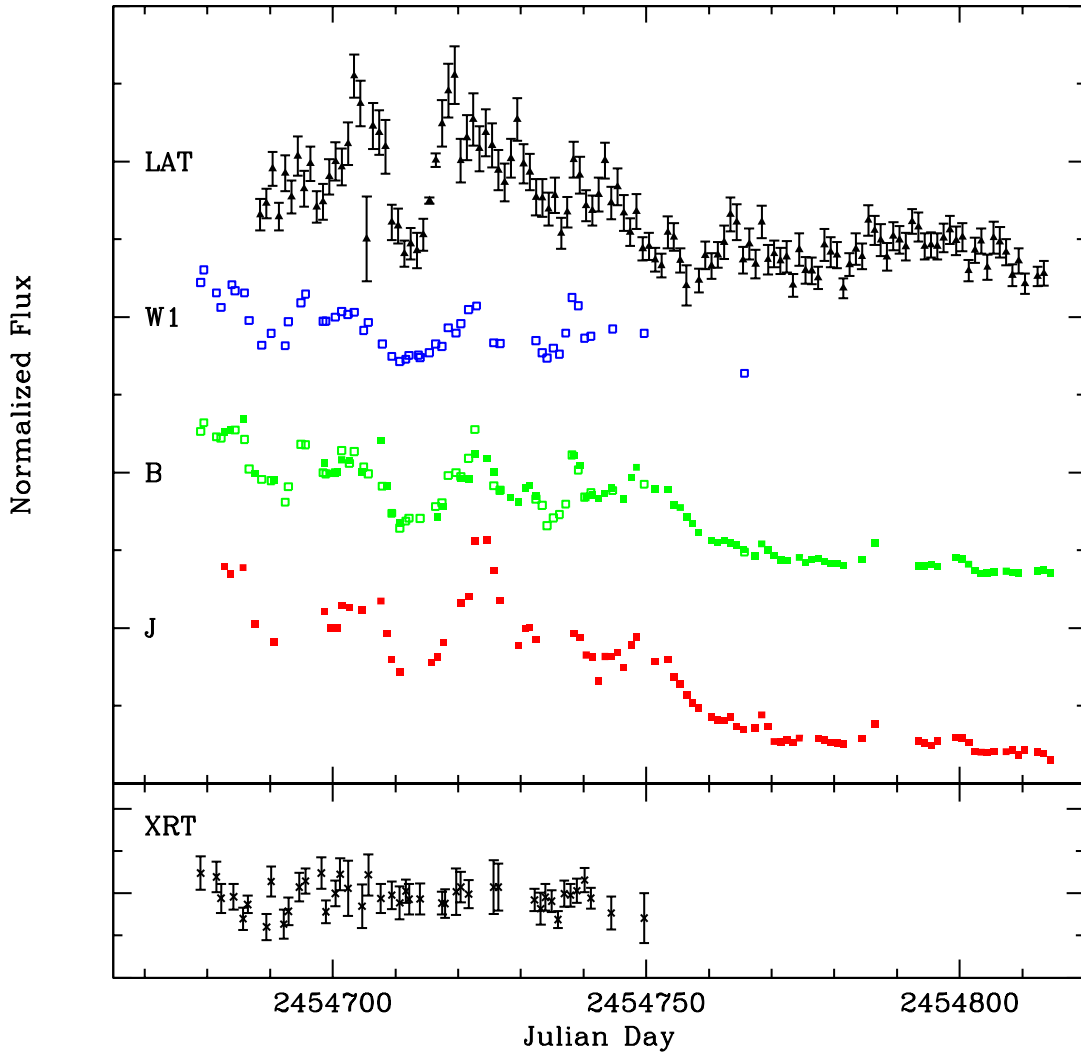


FIG. 1.— Multi-wavelength light curves of 3C 454.3 at (*top panel*) gamma-ray (0.1–300 GeV), UV (W1), optical (B), and IR (J) wavelengths from Fermi LAT, Swift UVOT, and SMARTS. Fluxes have been normalized to JD 2454700. Light curves are offset for clarity; minor tick spacing corresponds to 50% change. Fluxes at JD 2454700 are 2.83×10^{-6} cts s^{-1} at 0.1–300 GeV, 1.64×10^{-11} erg s^{-1} cm^{-2} in W1, 2.21×10^{-11} erg s^{-1} cm^{-2} in B, and 3.62×10^{-11} erg s^{-1} cm^{-2} in J. (*Bottom panel*) Swift XRT 2–10 keV light curve, normalized to flux at JD 2454700 (2.90×10^{-11} erg s^{-1} cm^{-2}). The IR/optical/UV variations are well correlated with the gamma-ray variations, with a lag of $\lesssim 1$ day, while the (minimal) X-ray variability is uncorrelated. The variability has much higher amplitude in the J-band than in B, which can be explained if there is an relatively constant blue component, as expected for an accretion disk. At $z=0.859$, Balmer continuum from an accretion disk, as well as Fe II and Mg II emission lines would be redshifted into the B and V bands; $H\alpha$ is shifted into the J band.

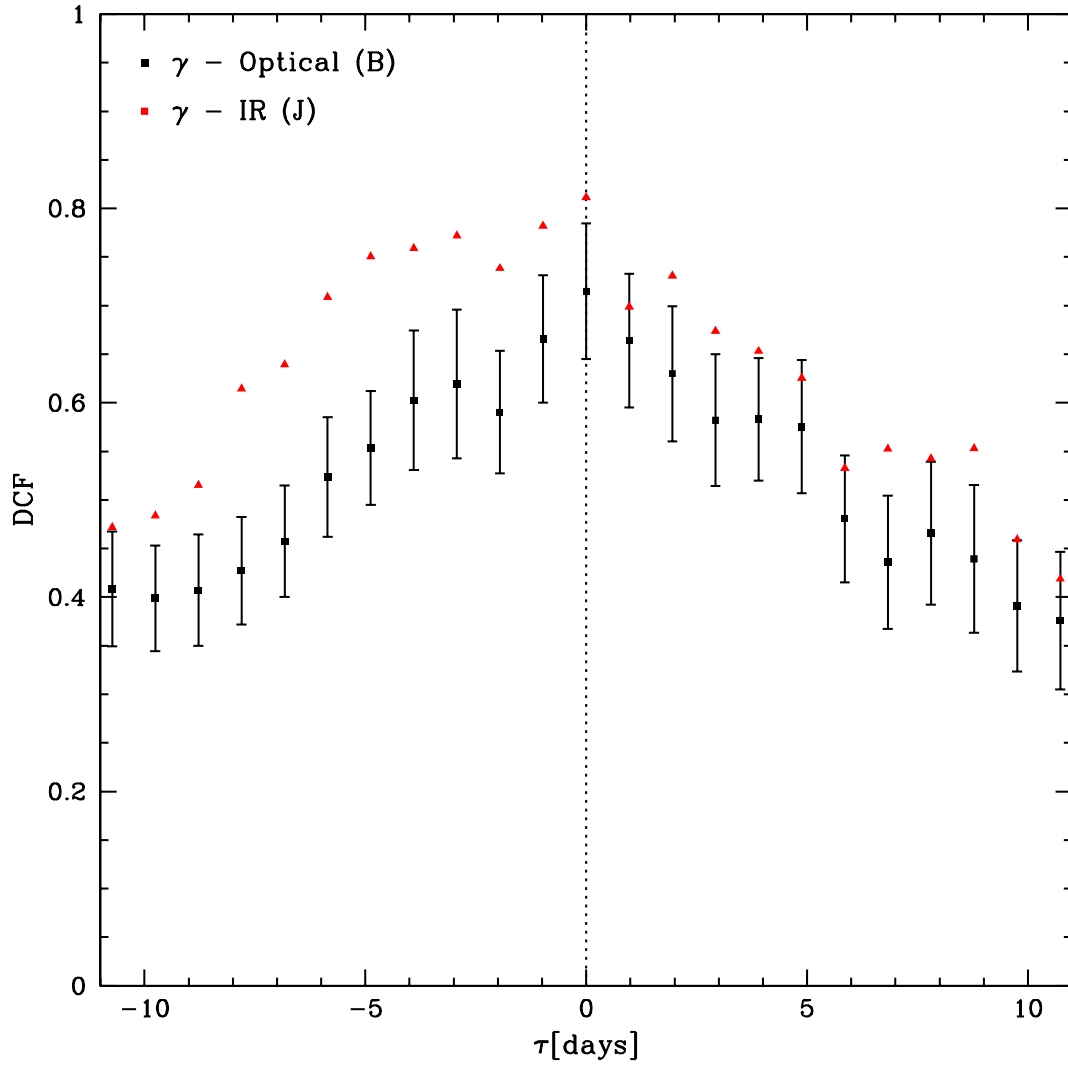


FIG. 2.— Discrete correlation function for optical B-band (black squares) and infrared J-band (red triangles) versus gamma-ray (0.1–300 GeV) light curves. Error bars on the γ - J-band DCF are comparable to the γ - B-band DCF and are omitted for clarity. The DCF peaks at zero lag, supporting external Compton models in which the variability is due to changes in the spectrum of relativistic electrons that both radiate the optical/IR synchrotron emission and up-scatter soft photons to GeV energies. The DCF has a hint of a shoulder at $\sim 3 - 5$ days (negative lags correspond to the gamma-rays *leading* the other band). This may result from slightly higher electron energies for the gamma-rays, which would give them shorter radiative timescales.

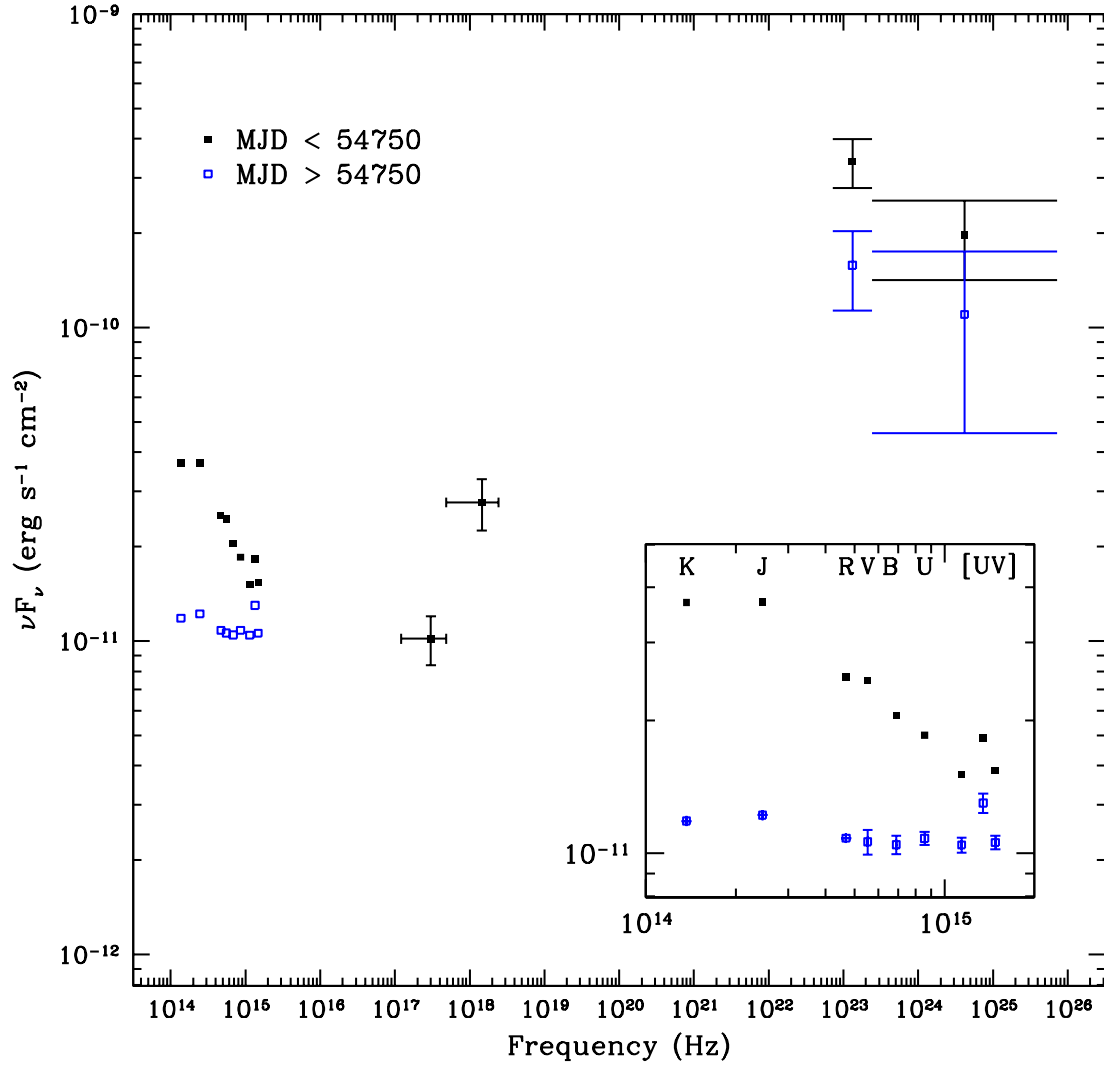


FIG. 3.— Spectral energy distributions for high (JD 2454680–2454750) and low (JD 2454750–2454820) states of 3C 454.3. Error bars not shown are smaller than the plotted points. Fermi/LAT fluxes are derived from the average count rate in the 0.3–1 GeV and 1–300 GeV bands assuming a power-law spectrum with photon index $\Gamma = 2$. The long-wavelength component in the low state is very flat, not unlike an accretion disk spectrum, while the variable component is clearly an infrared-bright jet.